

JEM–X: The X-ray monitor aboard INTEGRAL[★]

N. Lund¹, C. Budtz-Jørgensen¹, N. J. Westergaard¹, S. Brandt¹, I. L. Rasmussen¹, A. Hornstrup¹, C. A. Oxborrow¹, J. Chenevez¹, P. A. Jensen¹, S. Laursen¹, K. H. Andersen¹, P. B. Mogensen¹, I. Rasmussen¹, K. Omø¹, S. M. Pedersen¹, J. Polny¹, H. Andersson², T. Andersson², V. Kämäräinen², O. Vilhu³, J. Huovelin³, S. Maisala³, M. Morawski⁴, G. Juchnikowski⁴, E. Costa⁵, M. Feroci⁵, A. Rubini⁵, M. Rapisarda⁶, E. Morelli⁷, V. Carassiti⁸, F. Frontera⁸, C. Pelliciani⁸, G. Loffredo⁸, S. Martínez Núñez⁹, V. Reglero⁹, T. Velasco⁹, S. Larsson¹⁰, R. Svensson^{10,★★}, A. A. Zdziarski¹¹, A. Castro-Tirado¹², P. Attina¹³, M. Gorìa¹³, G. Giulianelli¹³, F. Cordero¹⁴, M. Rezaad¹⁴, M. Schmidt¹⁴, R. Carli¹⁵, C. Gomez¹⁵, P. L. Jensen¹⁵, G. Sarri¹⁵, A. Tiemon¹⁵, A. Orr¹⁵, R. Much¹⁵, P. Kretschmar¹⁶, and H. W. Schnopper¹⁷

¹ Danish Space Research Institute, Juliane Maries Vej 30, 2100 Copenhagen Ø, Denmark

² Metorex International Oy, Nihtisillankuja 5, PO Box 85, 02631 Espoo, Finland

³ Observatory, PO Box 14, 00014, University of Helsinki, Finland

⁴ Space Research Center, Bartycka 18A 00-716, Warsaw, Poland

⁵ Istituto de Astrofisica CNR, via del Fosso del Cavaliere 100, 00133 Rome, Italy

⁶ ENEA-Frascati UTS-Fusione, via Enrico Fermi 45, 00045 Frascati, Italy

⁷ IASF-Bologna, via Gobetti 101, 40129, Bologna, Italy

⁸ Dipartimento di Fisica, University of Ferrara, via del Paradiso 12, 44100 Ferrara, Italy

⁹ GACE, University of Valencia, PO Box 20085, 46071 Valencia, Spain

¹⁰ Stockholm University, Roslagstullgatan 21, Stockholm, Sweden

¹¹ Copernicus Astronomical Center, Bartycka 18, 00-716, Warsaw, Poland

¹² Instituto de Astrofísica de Andalucía (IAA-CSIC), PO Box 03004, 18080 Granada, Spain

¹³ Alenia Spazio, Space Division, Corso Marche 41, 10146 Torino, Italy

¹⁴ ESOC, Robert-Bosch Str. 5, 64293 Darmstadt, Germany

¹⁵ ESTEC, Keplerlaan 1, Postbus 299, 2200 AG Noordwijk, The Netherlands

¹⁶ MPI Extraterr. Physik, Gießenbachstr., 85748 Garching and ISDC, Chemin d'Écogia 16, Versoix, Switzerland

¹⁷ Harvard–Smithsonian Center for Astrophysics, 60 Garden Street, MA 02138, USA

Received 15 July 2003 / Accepted 3 September 2003

Abstract. The JEM–X monitor provides X-ray spectra and imaging with arcminute angular resolution in the 3 to 35 keV band. The good angular resolution and the low energy response of JEM–X plays an important role in the identification of gamma ray sources and in the analysis and scientific interpretation of the combined X-ray and gamma ray data. JEM–X is a coded aperture instrument consisting of two identical, coaligned telescopes. Each of the detectors has a sensitive area of 500 cm², and views the sky through its own coded aperture mask. The two coded masks are inverted with respect to each other and provides an angular resolution of 3' across an effective field of view of about 10° diameter.

Key words. instrumentation: detectors – X-rays: general

1. Introduction

The primary instruments of the INTEGRAL mission (Winkler et al. 2003) are designed for detailed studies of celestial objects in the gamma ray region of the electromagnetic spectrum between 20 keV and 10 MeV.

Send offprint requests to: N. Lund, e-mail: nl@dsri.dk

* Based on observations with INTEGRAL, an ESA project with instruments and science data centre funded by ESA member states (especially the PI countries: Denmark, France, Germany, Italy, Switzerland, Spain), Czech Republic and Poland, and with the participation of Russia and the USA.

** Deceased.

To obtain a more complete picture of the physical conditions in the observed sources, it is important to have simultaneous observations at both X-ray and optical wavelengths. The INTEGRAL payload is therefore augmented by an X-ray monitor, JEM–X, and an optical monitor, OMC. The JEM–X monitor was built by a collaboration of laboratories from Finland, Italy, Spain, Poland, Sweden and Denmark; the project was managed and lead by the Danish Space Research Institute (Schnopper 1996). JEM–X provides spectral data in the 3–35 keV band and also provides arcminute imaging to separate the contributions from sources in confused regions. The photon detection system consists of two identical imaging Microstrip Gas Chambers that view the sky through

Table 1. JEM–X main characteristics. (Quoted sensitivities are actual values for two JEM–X units.)

Mask diameter	535 mm
Detector diameter	250 mm
Mask–detector distance	3 401 mm
Energy–range	3–35 keV
Energy resolution	$\frac{\Delta E}{E} = 0.40 \times \left(\frac{1}{E[\text{keV}]} + \frac{1}{60} \right)^{1/2}$
Angular resolution	3.35'
Field of view (diameter)	4.8° Fully coded 7.5° Half response 13.2° Zero response
Point source location	15" (for a 10σ source)
Narrow line detection sensitivity	1.9×10^{-5} phot cm ⁻² s ⁻¹ @ 6 keV
Isolated on–axis source	8.5×10^{-5} phot cm ⁻² s ⁻¹ @ 30 keV
For a 3σ detection in a 10^6 s observation	
Continuum sensitivity	1.2×10^{-5} phot cm ⁻² s ⁻¹ keV ⁻¹ @ 6 keV
Isolated on–axis source	1.3×10^{-5} phot cm ⁻² s ⁻¹ keV ⁻¹ @ 30 keV
For a 3σ detection in a 10^6 s observation	
Time resolution	122 μ s

coded aperture masks. The main characteristics of JEM–X are listed in Table 1. Technical details of the JEM–X detector have been described by Kämäräinen et al. (1997) and by Budtz-Jørgensen et al. (1997). The details for the mask can be found in Ballesteros (1997).

2. Coded mask

The mask unit is shown in Fig. 1. The code patterns on the masks for two JEM–X units are identical but the masks are turned 180° with respect to each other to minimize common side lobes in the imaging process. The code is a hexagonal, uniformly redundant array pattern based on the biquadratic residue set for the prime number 22 501 (Baumert 1971). The code is cut in a 0.5 mm thick tungsten plate using electro-discharge wire cutting which provides an accuracy of 0.01 mm. The mask achieves opacities of 99.9% across the full energy range. The diameter of the coded area is 535 mm and the separation between neighboring hexagon elements is 3.3 mm (center to center). The mask/detector distance and mask element size defines the instrument angular resolution of 3.35 arcmin.

The basic mask pattern is about twice as large as the detector window, and therefore we do not have noise free coding. However, the sidelobes in the sky images are minimal with this design.

Following in't Zand et al. (1994) we have chosen, 25%, a rather small value, for the open fraction in order to achieve better source separation in crowded fields and also in an effort to reduce the background – and to save telemetry, which is scarce on INTEGRAL. An added advantage of the small open fraction is that the mask is almost fully interconnected and needs only a minimal amount of external support structure.

The tungsten mask membrane is suspended under tension from a peripheral titanium ring. A light titanium

structure supports the mask membrane from both sides. The loss of transparency due to this structure is 8% for on-axis sources (Reglero 2001). The total mass of each mask is 5.8 kg. The masks were manufactured in Spain by SENER under the supervision of the University of Valencia. The environmental tests on the completed mask units were carried out at INTA near Madrid.

3. The JEM–X detector unit

The JEM–X detector is a Microstrip Gas Chamber with a sensitive area of nominally 500 cm². The complete detector unit is shown in Fig. 3.2, and a cut-away drawing of the detector with its main components is shown in Fig. 3.2. The detector is assembled from the following modules: the detector vessel, the window, the collimator and the Microstrip sensor package with the associated electronics. The filling gas is a mixture of xenon (90%) and methane (10%) at 1.5 bar pressure.

Three flight detector units have been assembled, two of which are now flying on INTEGRAL. The third unit is used as a reference on-ground.

3.1. Detector structure

The detector body is made of stainless steel and consists of two parts, the mainframe and the cover welded together by electron beam welding. No gaskets are used in the construction. The cover is formed from a 2 mm thick stainless steel plate.

The mainframe is a cone shaped ring with a circular opening for mounting the collimator. The gas filling tubes, signal connectors and high voltage feed troughs are welded to this mainframe. All the internal components are also fixed to the mainframe. The internal structure consists of two sets of vertical studs and a spider structure carrying the microstrip sensor



Fig. 1. The JEM–X mask with its support structure.

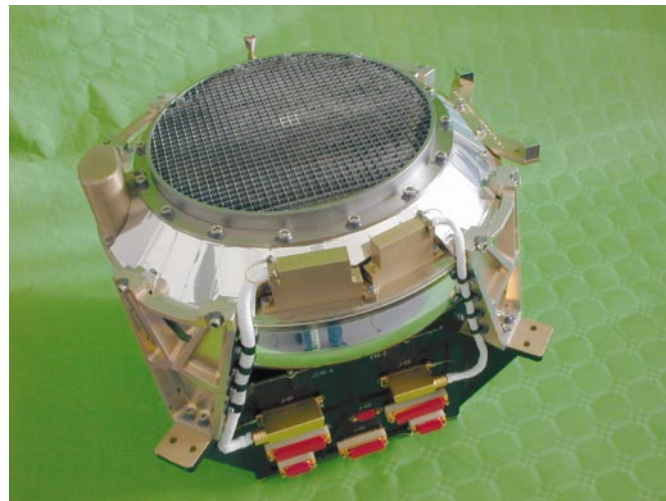


Fig. 2. Complete JEM–X unit, with DFEE electronics box.

package and the 36 pre-amplifiers. The spider is mounted on one set of studs and the other set carries the field forming rings. The detector mechanics has been manufactured by Metorex International OY as the technical contractor of the University of Helsinki. The detector assembly was carried out jointly by Metorex and DSRI.

3.2. Collimator

The collimator has a dual role as it acts as a support for the thin X-ray window against the internal pressure of the detector, and defines the field of view. The full-width-at-half-maximum of the collimator is tailored to have the same zero response as that of the detector-mask combination (6.6° FWHM). The collimator cell geometry is square. The core material of the collimator is molybdenum with a thickness of $180\ \mu\text{m}$. This provides an effective collimation for energies up to 60 keV. To reduce the molybdenum fluorescence background a $35\ \mu\text{m}$ layer of copper covers both sides of the cell walls. Finally, a $100\ \mu\text{m}$ aluminum layer is added on top to reduce the 8 keV fluorescence photons from the copper.

The open area of each cell in the collimator is $6.6 \times 6.6\ \text{mm}^2$ and the height of the cells is 57 mm. The on-axis open fraction is 85%. The collimator mass is about 4.7 kg. The collimator has been manufactured by Plansee AG under supervision of the University of Ferrara and Alenia Spazio.

3.3. X-ray entrance window

The detector window is a $250\ \mu\text{m}$ thick beryllium foil. The window is supported against the internal pressure by the collimator structure. The window is glued to a stainless steel mounting ring, which is welded to the detector mainframe. The window is electrically conductive and maintained at ground potential together with the rest of the detector body.

3.4. Microstrip sensor package

The microstrip plate is mounted on a support structure together with pre-amplifiers and high voltage distribution circuits.

The microstrip pattern is shown schematically in Fig. 4. The pattern is shaped as a regular octagon with a diameter of 292 mm. The 255 narrow anode strips and the 256 wider cathode strips alternate with a 1.062 mm pitch. The electrode dimensions can be found in Fig. 4. The strips are formed by a $0.2\ \mu\text{m}$ thick chromium layer sputtered on the glass substrate, (D 263 glass, Schott Glas AG). The microstrip plates were designed by DSRI and manufactured by IMT AG, Switzerland. The cathode strips are connected to the capacitive readout chains (RC Boards in Fig. 3.2) by wedge bonding via gold plated bond pads on the cathodes. The RC-chains connect each cathode strip to the neighboring strips via 2.2 nF capacitors and $1\ \text{M}\Omega$ resistors. The signals are picked up by 11 pre-amplifiers distributed along the capacitive chain.

One coordinate of the photon interaction point is determined from the centroid of the avalanche charge detected by the cathode pre-amplifiers. The orthogonal coordinate is obtained from a set of pickup electrodes on the backside of the glass plate. The backside electrodes are arranged on a 2 mm pitch and read out through capacitive chains by 20 pre-amplifiers.

The anode strips are connected into four groups connected to four separate pre-amplifiers. The signals from the anode groups are later combined and the sum signal is used for event triggering, energy determination and as input for the pulse shape analysis.

The microstrip plate is located 55 mm below the detector window. The detector requires two voltages in order to operate. The first is the drift voltage applied between the detector window (at ground potential) and the cathode strips on the plate. The second voltage is the gas-gain voltage. This voltage is applied between the anode and the cathode strips and controls the electron gas multiplication which take place immediately above the narrow anode strips.

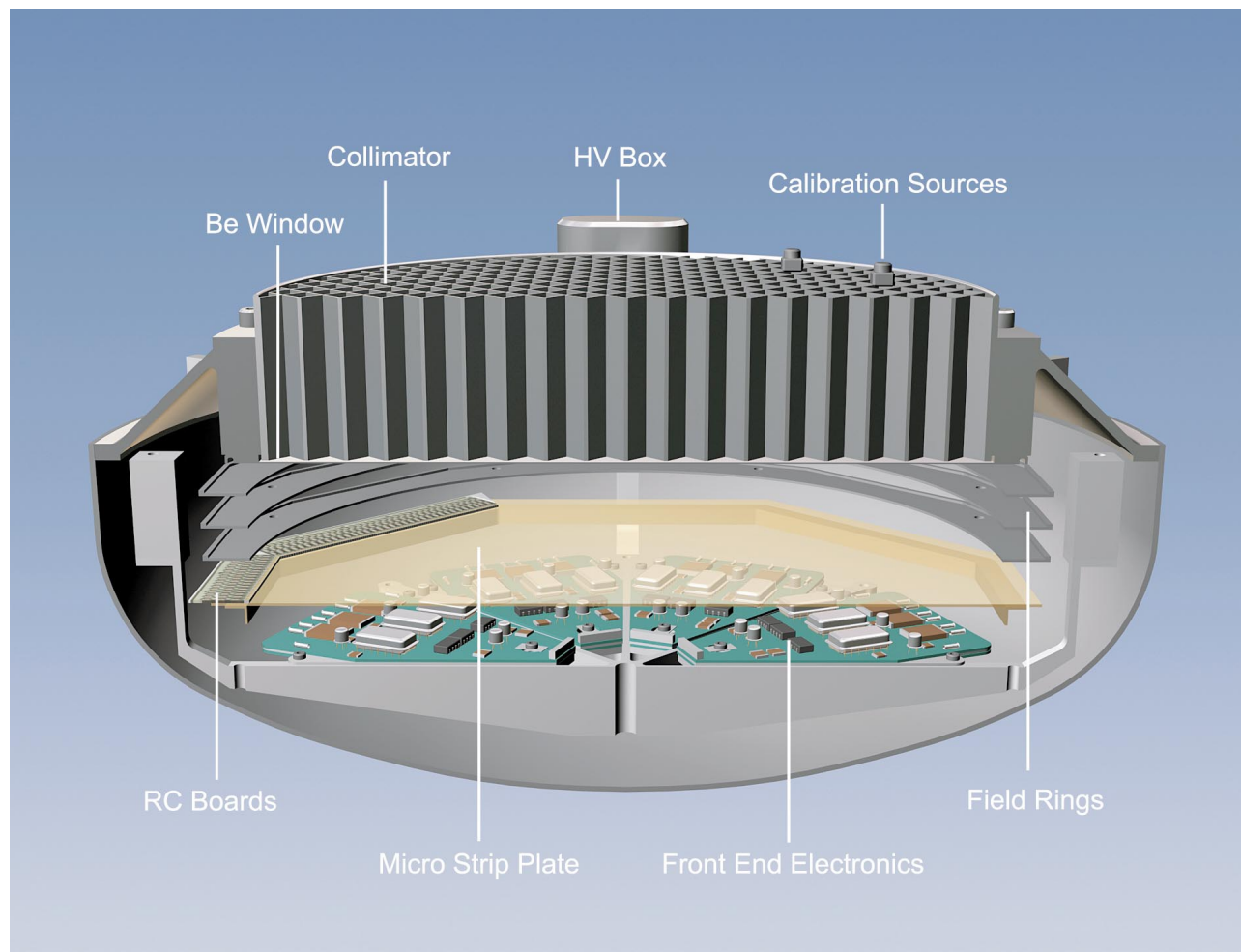


Fig. 3. Cut-away drawing of the JEM–X detector. The window diameter is 250 mm, the gas depth in the drift region is 55 mm.

3.5. Background rejection

A major source of background in space are cosmic ray particles which traverse the detector at a rate of 1500 s^{-1} . Due to the limitations of telemetry it is imperative to reject these events very efficiently on-board.

Particles entering through the side are rejected by the signal they deposit on a veto electrode surrounding the backside electrode pattern.

Particles which enter through the top or bottom are rejected by a pulse shape analysis technique, (Budtz-Jørgensen et al. 1994). The rejection efficiency for these events is augmented by using a “footprint” evaluation. Particles traversing the detector at inclined angles deposit charge on a large number of cathode or backside strips and can be distinguished from X-rays which deposit charge on only a few strips. The particle rejection is done on-board in software and is controlled by a number of adjustable parameters.

The particle rejection algorithm has performed well after launch, but requires careful tuning. The observed count rate of events after background rejection is only about 2% of the incident cosmic ray particle count rate. And the majority of the accepted events are actually real X-rays, not particle events leaking through the selection. The diffuse sky background alone

account for one quarter of the accepted events, and there are several background lines in our spectra which reveal an X-ray origin of these events. On this basis we estimate the rejection of signals due to penetrating particles to be about 99.5% efficient.

The particle rejection algorithm unavoidably also rejects a small fraction of the real X-ray events. This loss of good events does vary somewhat as function of energy, and at the moment we rely on observations of the Crab to fine tune our response function.

3.6. Radioactive calibration sources

The calibration system is composed of four collimated ^{109}Cd sources with a nominal strength of $25 \mu\text{Ci}$ (October 2002). The sources are placed within four cells of the collimator, and shielded by tubes of gold and molybdenum. Each source emits photons at 22, 25 and 88 keV. Additionally fluorescence photons at 7.5 and 8.3 keV from thin Ni windows covering the sources are present. The source units were provided by IASF, Rome. For technical reasons two of the Cd sources for JEM–X1 had to be substituted by ^{55}Fe sources emitting 5.9 keV photons.

Calibration spectra are accumulated every 256 s and transmitted to the ground as part of the instrument housekeeping data.

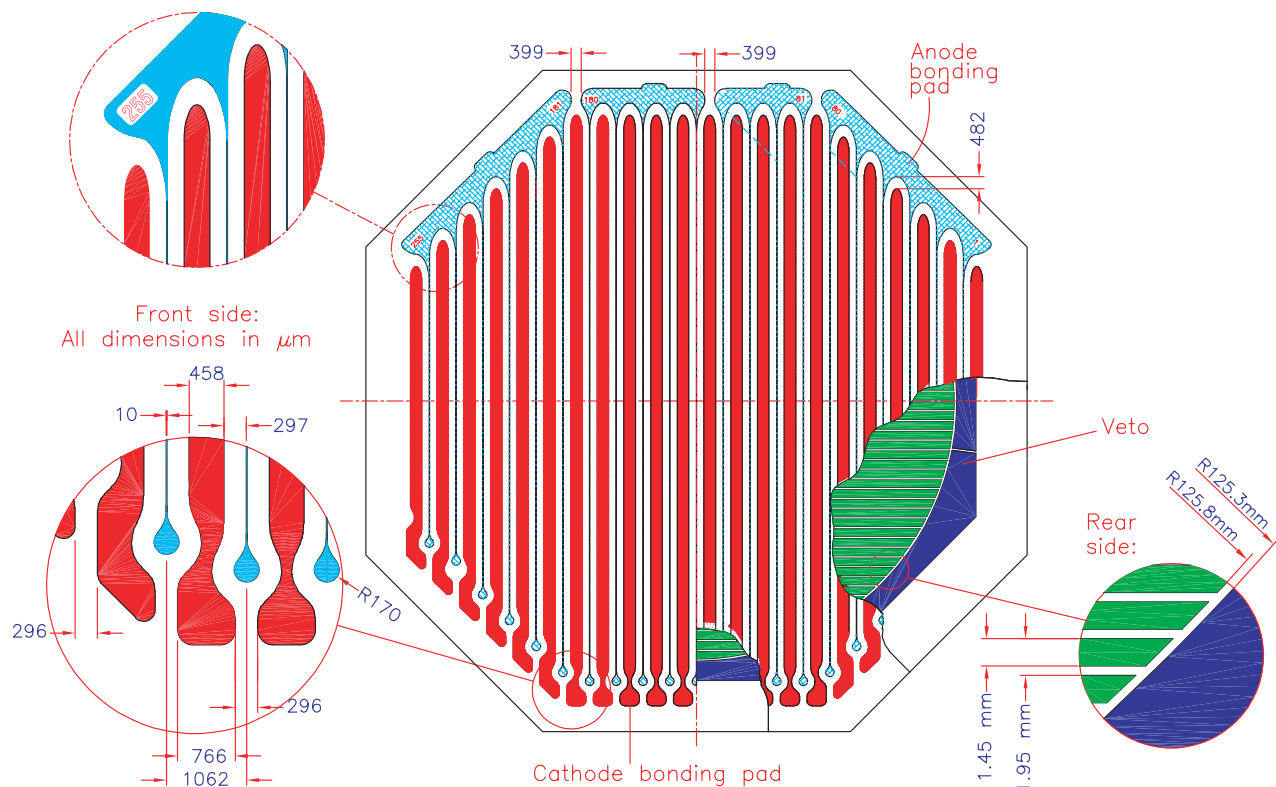


Fig. 4. Schematic drawing of the JEM–X Microstrip plate. Dimensions are in μm .

The calibration system is used to monitor time variations of the gas gain. This is important especially during the first few hours after the high voltage has been switched on. During this period the microstrip gain decreases by 25%. The gain is also affected by the detector temperature by about 1% per $^{\circ}\text{C}$.

The rapid initial decrease of the microstrip gain after application of the high voltage is a known effect and was seen in the JEM–X detectors prior to launch. The effect is attributed to surface polarization following application of electrical potentials between the electrodes (see Bouclier et al. 1995).

When operated for long times in the space radiation environment the start-up gain change decreases – as if there is a memory effect in the glass. (Brandt et al. 2003). This effect is currently under study in the laboratory – we can reproduce the evolution of the gain using a strong beta source, but no definite conclusion is available today concerning the mechanism causing these long term trends.

3.7. Electronics

The amount of electronics enclosed inside the detector gas volume is substantial. In addition to the RC-boards glued to the edge of the microstrip plate there are 36 pre-amplifiers and a number of low and high voltage distribution circuits. All internal electronics are mounted on ceramic circuit boards.

The instrument electronics outside the detector are divided into two units, one unit (the “DFEE”) which is specific for JEM–X, and another unit (the “DPE”) which is similar for all the instruments on INTEGRAL. The DPE’s were provided by ESA.

The DFEE incorporates a low voltage power supply, a dual high voltage unit, 4 boards with the amplifier chains for the detector signals, a housekeeping board, and a CPU board. All the electronics with exception of the high voltage unit was built at DSRI. The HV unit was built by CAEN SpA under supervision of IASF, Rome.

The timing of the analog event processing is controlled by an FPGA (Field Programmable Gate Array). The FPGA also monitors the trigger rate from the detector and will switch off the high voltage unit in case of very high count rates.

4. On-board software

The JEM–X on-board software is divided into two parts: one operating in the DPE and one in the DFEE environment. In both units the CPU is a 1750 compatible processor operating at 16 MHz. The choice of this processor, despite its limited performance, was dictated by the harsh radiation environment on INTEGRAL and the 5 year design lifetime requirement.

The DFEE part receives the digitized detector signals, performs the event analysis and transmit the event summary data (position, energy and time) for all accepted X-ray events. Most of the triggers received by the DFEE are due to cosmic ray protons and heavier nuclei, and more than 99% of these are rejected. The DFEE transmits housekeeping data to the DPE every 8 s. The DFEE also controls the instrument hardware – it switches on and off the high voltage unit and adjust the voltage and discriminator levels according to commands received from the DPE. The most complex part of the DFEE software is the event analysis which has two main tasks: elimination of

the huge background of particle induced triggers, and, for accepted events only, the determination of the X - and Y positions according to the 36 signals received from the detector. During normal operations, only the energy, the X - and Y -positions and the time stamp for the accepted events are transmitted from the DFEE to the DPE. The transfer takes place up to 8 times per second in blocks of ≈ 700 events. The software for the DFEE was developed at DSRI.

The DPE part receives the blocks of events from the DFEE and stores these in a buffer capable of holding 60 000 events. It then formats the data for transmission to the ground according to the data format specified for the observation. If events are received at a higher rate than can be transmitted the buffer will gradually fill up. When the buffer filling exceeds 50% the DPE will command the DFEE to activate the “grey filter” mechanism. This mechanism will discard, according to a pseudo-random scheme, a fraction of the events at the input to the DFEE. The event formatting and the control of the DFEE according to the contents of the “Broadcast Packet” are the most complex parts of the DPE software. The Broadcast Packet is transmitted from the satellite to the instruments every 8 s, it contains information about the status of the satellite (stable pointing, slewing, radiation environment, eclipse entry and exit etc.).

The DPE maintains an updated list of parameter changes and code corrections for the DFEE software. These data allows to restore operations relatively easily after a temporary switch-off, required for instance due to an eclipse situation. The software for the DPE was developed at the Space Research Centre in Warsaw.

5. Electrical ground support equipment

Corresponding to the division of the on-board electronics into an instrument specific part and a common part, also the electrical ground support equipment was divided into two: the Satellite Interface Simulator supplied by ESA, and the Instrument Station developed by the JEM–X project. The Instrument Station has been used for instrument development, checkout and calibration. The JEM–X Instrument Station was designed and built by the Space Research Centre in Warsaw. The station is capable of controlling and monitoring the DFEE and detector part of JEM–X without the involvement of the DPE. The software for the Instrument Station can collect data directly from the instrument or via the telemetry chain and provides a flexible graphical user interface to investigate the data in real-time during tests and during the early stages of the flight.

The Instrument Stations continues to be used for instrument calibration and verification in flight.

6. Tests and calibration

6.1. Detector cleanliness considerations

It was known during the early design phase that xenon based gas detectors are very susceptible to contamination by water, oxygen and electronegative gases, leading to rapid degradation of the energy resolution (Ramsey et al. 1988). Therefore it was

initially a serious concern that any electronics mounted inside the active detector volume would contaminate the counter gas and lead to degraded detector performance. However, keeping the electronics out of the gas volume would have required a very large number of high voltage feedthroughs and this was deemed to have been more complicated.

An elaborate programme of component testing was consequently carried out, in which all the components to be used inside the detector were tested for outgassing by actually placing them inside small, sealed, xenon filled detectors and monitoring the performance of these detectors over several years. These tests verified that the components by themselves would not contaminate the detector gas.

The materials used during the mounting of the ceramic circuit boards was another potential source of outgassing components, however, after intensive cleaning and baking of the completed boards and all other internal parts the gas contamination problem appears not to be an issue.

However, eliminating particulate contamination from the microstrip and electronics package turned out to be very difficult and critical, causing much agony, delay and concern during the assembly process. Microstrip detectors, because of the presence of the glass substrate between the electrodes and the very small distances between electrodes with large voltage differences are extremely vulnerable to short circuits caused by small metallic particles. Such particles are easily liberated during any mechanical handling or assembly process involving metallic screws, washers or tools. Proper choice of materials (no aluminium), good surface finish on all parts, careful cleaning and a very carefully planned and executed assembly process are all key requirements for achieving a working detector.

The final cleaning action was the bakeout under vacuum of each detector after the assembly in order to remove water and other outgassing components. The detectors were evacuated and baked for 3 weeks at a temperature of 80 °C before being filled with the xenon + 10% methane mixture at 1.5 bar and sealed off.

From the observed resolution of the calibration spectra there are no signs of gas degradation since the assembly of the two JEM–X flight detectors. This statement covers one year prior to launch up to the time of writing, 9 months into the flight

6.2. Stability of the microstrip electrodes

The fine anode strips on the microstrip plate are fragile and may be damaged if an electrical discharge is produced in the strong field around the anode strip. Such discharges may be produced by sufficiently strong local ionization of the gas – for instance caused by the traversal of a spallation fragment from a nuclear interaction or an ultra-heavy cosmic ray nucleus (see Hott 1998; Peskov et al. 1998). This effect limits gas gain for which the microstrip plate can be safely operated.

Prior to the detector assembly we conducted a number of measurements using an α -particle source ^{241}Am inserted in the active detector volume to simulate the cosmic ray bombardment in space. From our tests it was concluded that the detector

filled with Xe/CH₄ mixture at 1.5 bar could be safely operated at least up to a gas gain of 1500. This result was supported by additional tests performed with a scattered proton beam at DESY in 1999.

The value 1500 was then chosen as the nominal gain for the detectors and all on-ground calibrations were performed at this gain. This gain was reached when the anode potential was 900 V above the cathode potential. Unfortunately, after the launch, it was discovered, that the microstrip anodes eroded severely under these conditions. During the first week of operations we lost about one anode per day per detector.

After reducing the detector gain by a factor 3 the damage rate has dropped to a level of about one anode lost per two months. This is low enough to safely assure a working detector even after more than 5 years.

At present the anode voltage is about 800 V above the cathodes, and the cathodes 1100 V above ground. The drift field between the window and the plate is effectively the cathode voltage plus $\approx 20\%$ of the anode–cathode voltage difference, corresponding to about 230 V/cm.

6.3. Instrument calibrations

The JEM–X detectors were calibrated at the X-ray facility at the University of Ferrara (Loffredo et al. 2003). This installation consists of an X-ray generator, a monochromator and a XYZ table on which the detector is mounted such that the whole detector area can be scanned by an X-ray beam. The useful energy range of this equipment is from 10 keV to 140 keV. An additional 5.9 keV beam was provided by a collimated ⁵⁵Fe source. Including also the Xe K-escape peaks in the analysis, it was possible to study the detector energy and position resolution down to 3 keV. The results of the calibration campaign are described in Westergaard et al. (2002).

A typical energy spectrum for the FM1 detector recorded with a beam energy of 40.15 keV is shown in Fig. 5. Besides the main line both the Xe K_α and K_β escape lines are clearly visible. The measured energy resolution during the ground tests obey a \sqrt{E} dependence with:

$$\frac{\Delta E_{\text{FWHM}}}{E} = 0.40 \times \sqrt{\frac{1}{E[\text{keV}]}} \quad (1)$$

where ΔE_{FWHM} is the FWHM of the energy resolution. Due to the “gain noise” (Brandt et al. 2003) observed in space the in-flight resolution is slightly worse and can be described by:

$$\frac{\Delta E_{\text{FWHM}}}{E} = 0.40 \times \sqrt{\frac{1}{E[\text{keV}]} + \frac{1}{60}}. \quad (2)$$

The gas gain varies smoothly over the microstrip plate with deviations of $\pm 10\%$. These variations have been mapped and corrections are applied in the post processing. It must be noted, however, that some of the JEM–X telemetry formats (Spectral-Timing format, Spectrum format and Timing format) does not transfer the position information to the ground. For these formats the useable spectral resolution is therefore degraded by the detector nonuniformities and the following formulae apply:

$$\frac{\Delta E_{\text{FWHM}}}{E} = 0.40 \times \sqrt{\frac{1}{E[\text{keV}]} + \frac{1}{7}} \quad (\text{JEM-X1}) \quad (3)$$

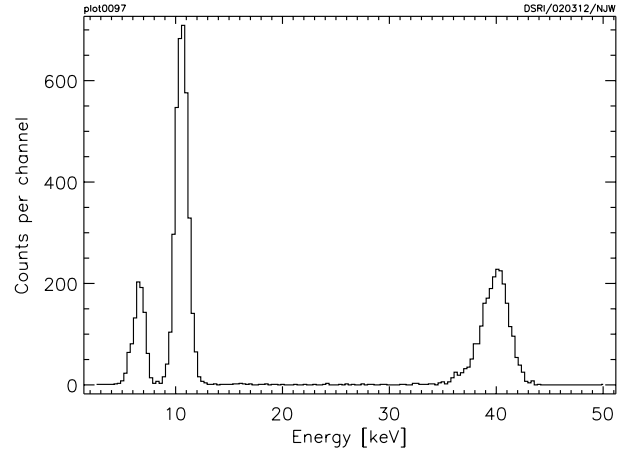


Fig. 5. A spectrum recorded with the FM1 detector for a beam energy of 40.15 keV. The K_α and K_β escape lines are clearly visible.

$$\frac{\Delta E_{\text{FWHM}}}{E} = 0.40 \times \sqrt{\frac{1}{E[\text{keV}]} + \frac{1}{9}} \quad (\text{JEM-X2}). \quad (4)$$

The measured detector position resolution at a gas gain of 1500 was 2.0 mm (FWHM) at 3 keV, had a minimum value of 0.5 mm between 10 to 20 keV and increased to 2 mm at 35 keV. The position non linearities of the detector response were determined making fine scans of the full active detector area with X-ray beams of 0.5 mm diameter. The scans were performed at 3 energies (5.9, 17 and 25 keV). Application of the derived position correction matrix reduced the systematic errors of the position determination to less than 0.2 mm.

In-flight the position resolution is reduced by about a factor two compared to the laboratory measurements due to the reduction in the gas gain. The position resolution is still adequate for image reconstruction and source spectrum extraction even at the lowest energies (Brandt et al. 2003).

6.4. Instrument efficiency

The efficiency of the JEM–X detector is shown in Fig. 6. Included in this calculation is the on-axis collimator transmission, the window transmission, the gas transparency and the effect of the on-board rejection of the majority of the X-rays with energies above the xenon K-edge. In most cases these X-rays are absorbed via a two stage process involving the initial absorption by interaction with an electron in the K-shell, and later the emission and reabsorption of a fluorescence photon. Such “two-point” events cannot be reliably localized and are therefore rejected on-board.

In space the above efficiency is somewhat reduced due to the deadtime associated with the handling of the intense particle background ($\approx 12\%$) and losses due to the on-board background rejection mechanism at lower energies.

In the derivation of the efficiency of the complete coded mask instrument it is necessary to consider also the decoding of the images, which involves a number of energy dependent effects, and at the present time we rely heavily on the calibration observations of the Crab in order to derive the instrument response function (Brandt et al. 2003).

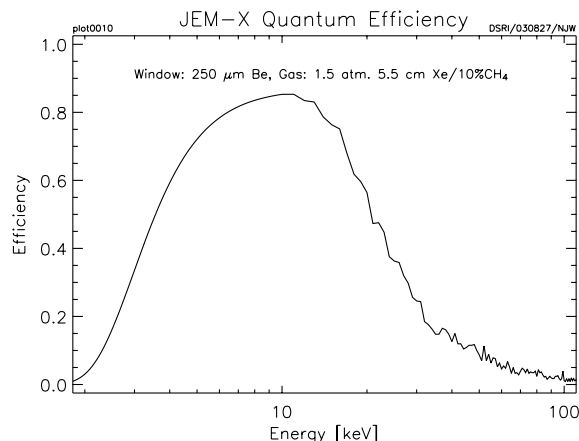


Fig. 6. JEM-X detector quantum efficiency (including the 85% transmission of the on-axis collimator).

7. Conclusion

The JEM-X instrument on INTEGRAL demonstrates for the first time the successful use of microstrip position sensitive X-ray detectors in space.

Early in the JEM-X development program the gas cleanliness issue, was considered the most serious limitation to the lifetime of the detectors. From the experience gained until now this seems not to be a major problem.

Significant delays were incurred in the assembly of the JEM-X detectors due to the difficulty of eliminating the small metallic particles resulting from the assembly process itself. We strongly recommend that this problem is carefully considered already in the design stage of any future experiment involving sealed microstrip detectors.

In the space environment, with the unavoidable background of ultra-heavy cosmic rays, our experience shows that the gas gain must be limited to a few hundred if anode erosion due to ionization induced discharges shall be avoided. A future design with individual readout circuits associated with each cathode and backside strip, could realize the full potential of the microstrip design for high spatial and energy resolution, even when operating with a very low gas gain.

In conclusion: The excellent results from the first 9 months of operation in space demonstrate that the JEM-X project has been successful and is now providing the INTEGRAL mission with an X-ray monitor matching the sensitivity and performance of the gamma-ray instruments.

Acknowledgements. The Danish Space Research Institute acknowledges the support given to the development of the JEM-X instrument from the PRODEX programme. Authors from the University of Helsinki Observatory acknowledge the Academy of Finland, TEKES, and the Finnish space research programme Antares for financial support of this research. A. A. Zdziarski has been supported by KBN grants 5P03D00821, 2P03C00619pl.2, PBZ-054/P03/2001 and the Foundation for Polish Science. The authors from Italy acknowledge the support of Agenzia Spaziale Italia. The Spanish contribution to JEM-X has been funded by CICYT.

References

- Ballesteros, F., Collado, V., Payne, B., et al. 1997, ESA SP-382, 659
- Baumert, L. D. 1971, Lecture Notes in Mathematics No. 182, Cyclic Difference Sets (Springer, Berlin)
- Bouclier, R., Capeans, M., Garabatos, C., et al. 1995, in Proc. of the International Workshop on Micro-Strip Gas Chambers, ed. G. Della Mea, & F. Sauli, 39
- Brandt, S., Budtz-Jørgensen, C., Lund, N., et al. 2003, A&A, 411, L243
- Budtz-Jørgensen, C., Bahnsen, A., Madsen, M. M., et al. 1994, Proc. SPIE, 2279, 517
- Budtz-Jørgensen, C., Westergaard, N.-J., Rasmussen, I. L., et al. 1997, in Proc. of the 2nd INTEGRAL Workshop., ed. C. Winkler, T. Courvoisier, & Ph. Durouchoux, ESA SP-382, March 1997, 651
- Feroci, M., Rapisarda, M., Costa, E., et al. 1999, Astro. Lett. and Comm., 39, 421
- Hott, T. 1998, Nucl. Instr. and Meth., A408, 258
- in't Zand, J. J. M., Heise, J., & Jager, R. 1994, A&A, 288, 665
- Kämäräinen, V., Andersson, H., & Andersson, T. 1997, in Proc. of the 2nd INTEGRAL Workshop., ed. C. Winkler, T. Courvoisier, & Ph. Durouchoux, ESA SP-382, March 1997, 655
- Loffredo, G., Pellicciari, C., Frontera, F., et al. 2003, A&A, 411, L239
- Peskov, V., Ramsey, B. D., & Fonte, P. 1998, IEEE Trans. Nucl. Sci., 45, 244
- Ramsey, B. D., Elsner, E. F., & Weisskopf, M. C. 1988, Nucl. Instr. and Meth., A270, 178
- Reglero, V., Rodrigo, T., Velasco, T., et al. 2001, in Proc. of the 4th INTEGRAL Workshop., ed. A. Gimenez, V. Reglero, & C. Winkler, ESA SP-459, September 2001, 623
- Schnopper, H. W., Budtz-Jørgensen, C., Westergaard, N. J., et al. 1996, Joint European X-Ray Monitor (JEM-X): X-ray monitor for ESA's INTEGRAL mission, in Gamma-Ray and Cosmic-Ray Detectors, Techniques, and Missions. ed. B.D. Ramsey, & T.A. Parnell, Proc. SPIE, 2806, 297
- Westergaard, N. J., Budtz-Jørgensen, C., & Lund, N. 2002, DSRI Technical Report IN-PL-JEM-007
- Westergaard, N. J., Kretschmar, P., Oxborrow, C. A. et al. 2003, A&A, 411, L257
- Winkler, C., Courvoisier, T. J.-L., Di Cocco, G., et al. 2003, A&A, 411, L1